A String-Current Behavior and Current Sensing Based Technique for Line-Line Fault Detection in Photovoltaic Systems

Wenchao Miao, K. H. Lam, and Philip W. T. Pong, *Senior Member, IEEE*

Department of Electrical and Electronic Engineering, The University of Hong Kong, Hong Kong

The normal operation of a photovoltaic (PV) system is undermined by Line-Line (LL) faults. A LL fault, which establishes an unintentional current path between two points of different potentials, can cause malfunctions and even fire hazards to the PV systems. Although the overcurrent protection devices such as fuses are utilized to terminate the LL faults, the maximum power point tracking (MPPT) controller, partial shading, and blocking diodes are affecting the fault currents and they may be lower than the rated current of the fuse. Therefore, it is necessary to develop an effective LL fault detection technique for PV systems. In this paper, a LL fault detection technique based on the string-current behavior and current sensing is proposed. The characteristics of LL faults and the string-current behavior under the various fault conditions were analyzed to develop the algorithm. The proposed technique could determine the occurrence, type, location, and percentage of the LL faults. It was verified that the fault detection algorithm and current sensors in specific locations could detect the LL faults effectively despite the effects of MPPT, partial shading, and blocking diodes.

***Index Terms*—Current sensing, line-line fault, photovoltaic systems, string-current behavior.**

I. Introduction

PHOTOVOLTAIC (PV) systems play an important role in renewable energies. At the end of 2019, the cumulative global capacity of PV systems estimated to reach 650 GW which is capable of generating approximately 4 % of the worldwide electricity demand [1]. However, the safety, reliability, and efficiency of a PV system are susceptible to electrical faults. In PV arrays, an unintentional current path between two points with different potentials is defined as a line-line (LL) fault. Undetected LL faults may induce catastrophic failures and lead to fire hazards [2]. Currently, the overcurrent protection devices (OCPDs) are commonly used to terminate the LL faults. Nevertheless, the LL faults cannot be eliminated by the OCPDs or other conventional protection devices due to the effects of maximum power point tracking (MPPT) controller, partial shading, and blocking diodes [3]. Therefore, a competent LL fault detection technique is essential for ensuing PV systems to operate reliably.

Although current-voltage (I-V) characteristics of PV modules can be used to diagnose the faults in a PV system [4, 5], it is difficult to obtain the I-V curves of PV modules during the operation of a PV system and the indicators depending on the operation points are not reliable. The operation points may be the same in LL faults and partial shading conditions since the MPPT keeps tracking the operation points to output maximum power. This problem also impacts the MPPT-based method for LL faults detection [6], and it is complicated to calculate the expected operation points for comparing with the real-time operation points under various conditions. The LL faults and partial shading can be differentiated by utilizing the array voltage, current, and irradiance [7] by the predefined thresholds which may vary with PV systems. Besides, they can be diagnosed by comparing the expected voltage, current, and power with the actual measurements [8]. However, it is difficult to acquire the percentage and location of LL faults.

Additionally, a health evaluation method is developed based on Gaussian mixture models and empirical mode decomposition to reflect the performance of PV systems [9] and computational complexity may be enlarged. There are fault diagnosis methods based on statistical analysis [10, 11], but numerous sets of data are required which incur extra costs in capturing and computing the data. The machine learning tools have been applied to classify and detect LL faults in PV systems [12-14], however, emulations of each fault conditions in the PV systems are obliged to attain the training data. To identify and locate the faults, a digital twin approach has been developed which requires an estimator in each PV module [15]. Though sensors are adopted in each PV module to detect and locate the faults [16], modifications of the systems are incurred. Thus, a cost-effective technique that is capable of detecting and locating LL faults in PV systems is demanded.

Furthermore, most of the previous research works have not considered the cases with blocking diodes which provoke different fault current and they are extensively used in PV systems to avoid the back-feeding current. In this paper, the effects of MPPT, partial shading, and blocking diodes on LL faults in PV systems are modeled and investigated with Simulink. A string-current behavior and current-sensing based technique is proposed for diagnosing and locating LL faults. The characteristics of LL faults and the string-current behavior are critical for developing a reliable fault-detection algorithm, For the first time, they are studied and analyzed under various fault conditions in this paper, leading to the development of a LL fault-detection technique that is applicable across PV arrays of different configurations. This technique based on the string-current behavior and current sensing has the unique advantage over the traditional techniques that the occurrence, type, location, and percentage of the LL faults can be determined in a convenient and low-cost manner. The cost-effective and compact magnetic sensors such as magnetoresistive (MR) sensors can be applied to measure the string current non-invasively [17, 18]. The proposed LL fault

The authors are with the Department of Electrical and Electronic Engineering, The University of Hong Kong, Hong Kong (e-mail: ppong@eee.hku.hk).

detection algorithm is validated with the simulation results. Hence, a convenient technique is developed in a low-cost and real-time manner to detect LL faults in PV systems despite the effects of MPPT, partial shading, and blocking diodes.

This paper is organized as follows. In Section II, the effects of MPPT, partial shading, and blocking diodes on LL faults and string-current behavior are elaborated. In Section III, the fault detection scheme is illustrated. In Section IV, the simulation and validation of the proposed technique are presented. The conclusion is drawn in Section V.

II. Principles of LL Fault and Analysis of String-Current Behavior

A. Characteristics of LL Fault

To investigate the performance of a PV system in fault conditions, the PV system consisting of three strings in which each has four series-connected modules (1STH-215-P, 1Soltech) is developed on Simulink. The MPPT controller with a boost converter is adopted. The potential faults in a string and between strings are depicted in Fig. 1. The LL1, LL2, and LL3 are 25 %, 50 %, and 75 % intra-string (IS) LL faults respectively. The LL4 and LL5 are 25 % and 50 % cross-string (CS) LL faults. The current of the PV string 1 (I_{PV1}) when 25 % and 50 % IS LL fault accidentally occur in the PV string 1 (PVS1) at 0.5 s is shown in Fig. 2 (a) respectively. The back-feeding current appears when OCPD is used in the string, but it can be inhibited by blocking diodes. The OCPD can terminate the back-feeding current when it is larger than the rated current of OCPD which is 2.1 times the short circuit current (I_{SC}) of PVS1 [3]. However, the back-feeding current is lower than the 2.1 × I_{SC} at the 25 % IS LL fault which may cause malfunction of the system and accelerate the degradation or even damage the PV modules. Thus, the blocking diodes are widely used in PV systems to suppress back-feeding current and considered in this paper.

The partial shading of 300 and 100 W/m^2 at the last module of PVS1, IS LL faults in PVS1, and CS LL faults between PVS1 and PVS2 are examined as shown in Fig. 1. The I-V and power-voltage (P-V) characteristics of the PV system under the three cases are shown in Fig. 2 (b), (c) and (d) respectively. Though the MPP varies with the partial shading and fault conditions, there are cases that the MPPs are the same resulting in difficulties to determine the type and location of faults. For example, the MPPs at partial shading of 100 W/m^2, 25 % IS LL fault, and 25 % CS LL fault are approximately the same. Besides, the MPPs of 50 %, 75 % LL faults, and 50 % CS LL fault are almost the same. Consequently, it is necessary to further analyze the characteristics of fault string current with the effects of MPPT, partial shading, and blocking diodes to develop a comprehensive algorithm for LL fault detection.

B. String-Current Behavior

The single IS LL faults and CS LL faults are researched to derive the string-current equations in each condition. In this way, the type, location, and percentage of a LL fault can be determined by using the string current. The single IS LL fault,

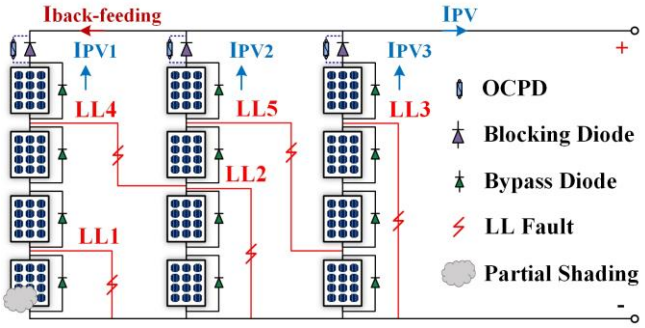

Fig. 1. The potential LL faults in the PV array with OCPD or bypass diode.

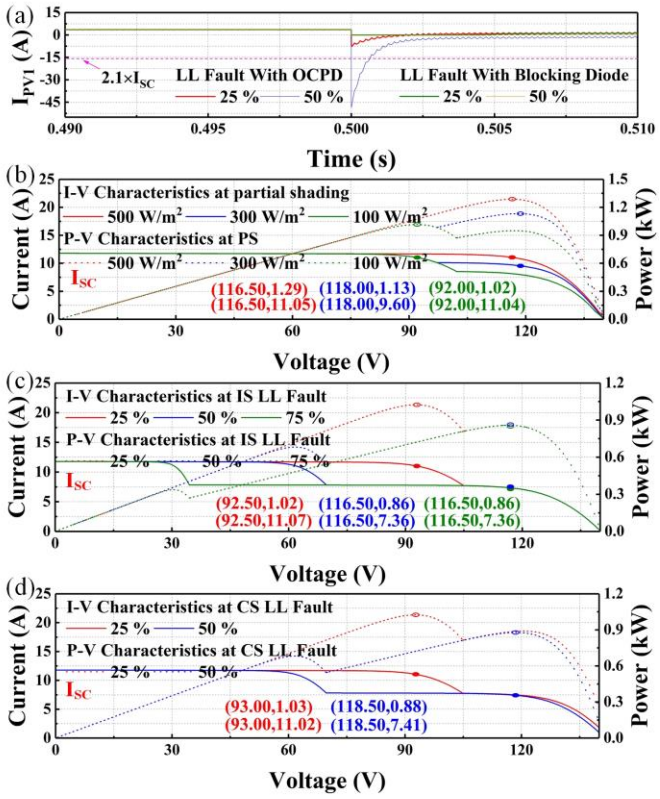

Fig. 2. The string current, I-V, and P-V characteristics of the PV system in fault conditions. (a) I_{PV1} at LL1 and LL2. (b) The effects of partial shading. (c) The effects of IS LL faults. (d) The effects of CS LL faults.

double IS LL fault, and single CS LL fault are considered. The multiple LL fault conditions such as double CS LL fault, which cause apparent fault current and I_{SC} in numbers of strings for detection, are different from the partial shading. Thus, they can be detected effortlessly and are not investigated in this research. When the single IS LL fault occurs, there are two possible cases that (I) the normal PV modules in the unhealthy string are working at voltage slightly larger than the voltage of MPP (V_m) and thus the current will be slightly lower than the current of MPP (I_m), and the voltage of the modules in healthy strings is lower than the V_m so that all modules are working at operation points close to the MPP to ensure the maximum power output or (II) the modules in healthy strings are working at MPP and the unhealthy string is open circuit since the voltage of unhealthy string reaches the open-circuit voltage in this case. The PV system operates in the case with larger power because the MPPT controller ensures the system to output the maximum power. For a PV

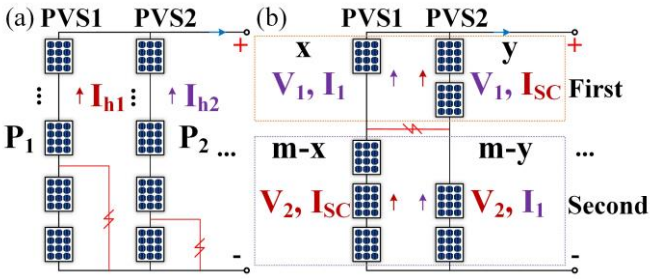

Fig. 3. The circuit diagram of the unhealthy strings in the CS LL fault.

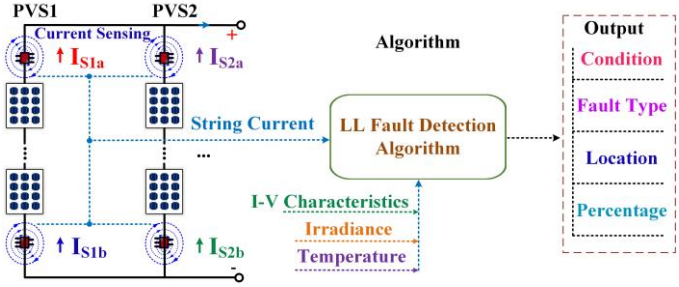

Fig. 4. The online LL fault detection scheme based on string-current behavior and current sensing by MR sensors.

array in size of row (m) × column (n) as depicted in Fig. 3 (a), the following equations can be derived to attain the percentage of normal modules of the unhealthy string (P) to achieve a higher power than case II. When the unhealthy string still works, the normal modules are operating at the operation point close to MPP due to MPPT controller. Thus, the voltage and current of the normal PV modules in the unhealthy string can be regarded as V_m and I_m.

$$V_m \times I_m \times m \times P + V_m \times m \times P \times I_h \times n^* \geq V_m \times I_m \times n^* \times m \quad (1)$$

where I_h is the current of the healthy string, n^* is the number of the healthy strings and it is n-1 in this case. Hence,

$$P \geq I_m \times n^* / (I_m + I_h \times n^*) \quad (2)$$

Since the voltage of the healthy string is lower than V_m, the current is close to I_{SC} which can be determined from the I-V characteristics of a PV module. This can also be observed from the I-V curve under 500 W/m^2 in Fig. 2 (b).

$$I_h \approx I_{SC} \quad (3)$$

Therefore,

$$P > n^* / ((I_{SC} / I_m) \times n^* + 1) \quad (4)$$

Similarly, when double IS LL fault happens as shown in Fig. 3 (a), the unhealthy strings are still working when the PV system generates more power with the unhealthy string of larger P operating at MPP than the case that the healthy strings operating at MPP and unhealthy strings are in open circuit. Thus, Eq. (5) can be derived.

$$V_m \times I_m \times m \times P_2 + V_m \times m \times P_2 \times I_{h1} + V_m \times m \times P_2 \times I_h \times n^* \geq V_m \times I_m \times n^* \times m \quad (5)$$

where P_2 is also the percentage of normal modules of the unhealthy string with single LL fault (P_2 is larger than P_1), I_{h1} is the current of the unhealthy string with P_1, n^* is n-2. Thus,

$$P_2 \geq n^* / ((I_{SC} / I_m) \times n^* + I_{h1} / I_m + 1) \quad (6)$$

Since the voltage of the unhealthy string with P_1 is larger than V_m, the current should be much lower than I_m. Therefore,

$$0 < I_{h1} \ll I_m \quad (7)$$

The unhealthy strings in the CS LL fault are shown in Fig. 3 (b). The x is the number of modules in the first part of PVS1 and y is the number of modules in the first part of PVS2. According to the configuration, the voltage of the first part of PVS1 (V_1) equals to the first part of PVS2. The voltage of the second part of PVS1 (V_2) equals to the second part of PVS2. Since x is smaller than y, the voltages of the first part of PVS2 and second part of PVS1 are lower than V_m and thus their currents are approximate to I_{SC}. The currents of the first part of PVS1 and the second part of PVS2 can be regarded as I_1. When the difference between y and x increases, the current I_1 decreases. The first part of PVS1 and the second part of PVS2 become open circuit when I_1 decreases to 0. When the CS LL fault occurs, the voltage of the modules in healthy strings is slightly lower than V_m due to the MPPT controller. The current I_h is approximate to I_m. Thus,

$$V_1 + V_2 \approx m \times V_m \quad (8)$$

$$I_h \approx I_m \quad (9)$$

The I_1 is non-zero only when the power generated with all modules in operation is larger than the power generated with parts of the unhealthy strings being open circuit. Hence, Eq. (10) can be derived.

$$2 \times m \times V_m (I_1 + I_{SC}) + m \times V_m \times I_h \times n^* \geq V_{OC} \times I_{SC} \times (y + m - x) + V_{OC} \times (y + m - x) \times I_h \times n^* \quad (10)$$

where V_{OC} is the open-circuit voltage of the PV module. Therefore,

$$y - x \leq \frac{2 \times m \times V_m \times (I_{SC} + I_1) + V_m \times I_m \times m \times n^*}{V_{OC} \times I_{SC} + V_{OC} \times n^* \times I_m} - m \quad (11)$$

According to the string-current behavior in each fault condition, the LL fault detection algorithm is developed with MATLAB based on the Eq. (4), (6), and (11). The current sensors can be installed on each string to measure the string current. In this way, the occurrence, location, and percentage of the LL faults can be estimated by inputting the string currents into the algorithm. A LL fault detection scheme based on this algorithm and current sensing can be developed to monitor the real-time condition of a PV system.

III. LL Fault Detection

The fault detection scheme can be developed as shown in Fig. 4. The current sensors (MR sensors) are placed on the beginning and terminal of each string to measure the string current. For instance, the current at the beginning of PVS1 (I_{S1a}), the terminal of PVS1 (I_{S1b}), the beginning of PVS2 (I_{S2a}), and the terminal of PVS2 (I_{S2b}) are attained as depicted in Fig. 4. The I-V characteristics of the PV module are defined in the algorithm so that the theoretical values of string current can be estimated. The irradiance and ambient temperature can be obtained from the weather station where the PV system is located. By inputting the string currents, irradiance, and ambient temperature to the algorithm, the LL faults can be diagnosed by using the distinct current features in various

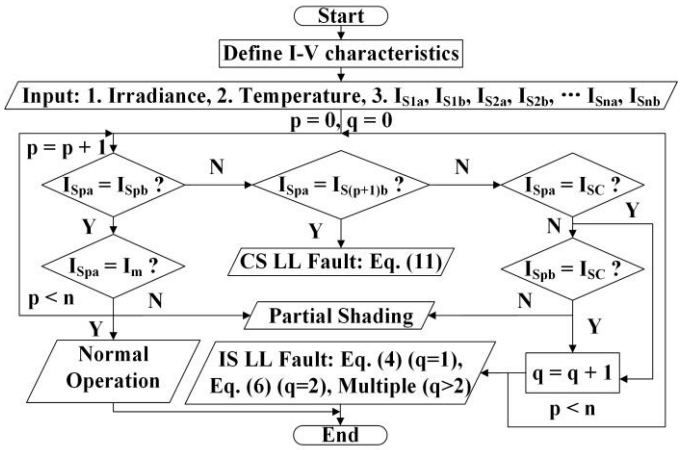

Fig. 5. LL fault detection algorithm.

conditions despite the effects of partial shading. The occurrence, type, location, and percentage of LL faults can be determined by the proposed algorithm. Since the MR sensors can measure the current non-invasively and they are placed on the surface of power cables, PV systems are not interfered. The harsh environment may impact the performance and lifetime of MR sensors. For protection, the MR sensors can be installed inside the PV array combiner box, where PV strings are merged together, to sense the current.

The proposed LL fault detection algorithm is illustrated in Fig. 5. Initially, the I-V characteristics of the PV modules are defined. The irradiance, temperature, and string currents are inputted to evaluate the condition of the PV system. The PV system is considered in the normal operation when the current of the beginning and terminal of each string is the same and equals to I_m. It is under partial shading when the current of the beginning and terminal of the string is the same and lower than I_m. The partial shading could also cause asymmetric string current due to the current passes through the bypass diode when the irradiance is too low to sustain the operation of the PV modules. However, there is no I_{SC} during the partial shading. The string current is asymmetric in the appearance of the CS LL fault and Eq. (11) can be used to calculate the number of mismatched modules. The IS LL fault can be detected when the current is asymmetric and I_{SC} is induced. The percentage of the IS LL fault can be estimated by Eq. (4) and Eq. (6). The multiple IS or CS LL faults can be detected effortlessly since they are causing apparent fault current in numbers of string and these situations rarely happen. Thus, they are not further investigated.

IV. Validation and Discussion

The proposed technique is validated with a PV system in a configuration of 8 (m) × 6 (n) which can generate power larger than 5 kW under the irradiance of 500 W/m^2 and the temperature of 25 °C. In this case, the I_{SC}, I_m, V_m, and V_{OC} can be obtained from I-V characteristics to be 3.93 A, 3.68 A, 29.33 V, and 35.22 V respectively. The LL faults in various conditions are emulated and the string currents are evaluated to verify the proposed technique. It is also demonstrated that the LL faults can be detected despite the effects of partial

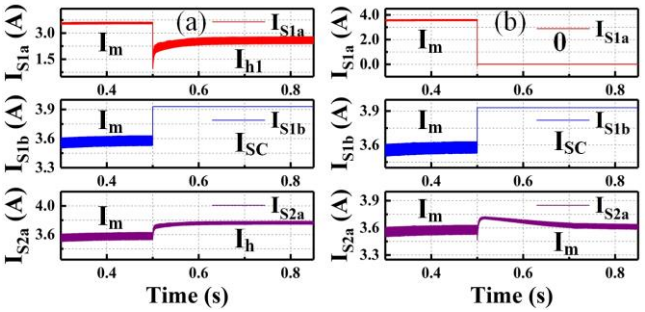

Fig. 6. The string current at the occurrence of (a) P is 87.5 % and (b) P is 75 % during IS LL faults.

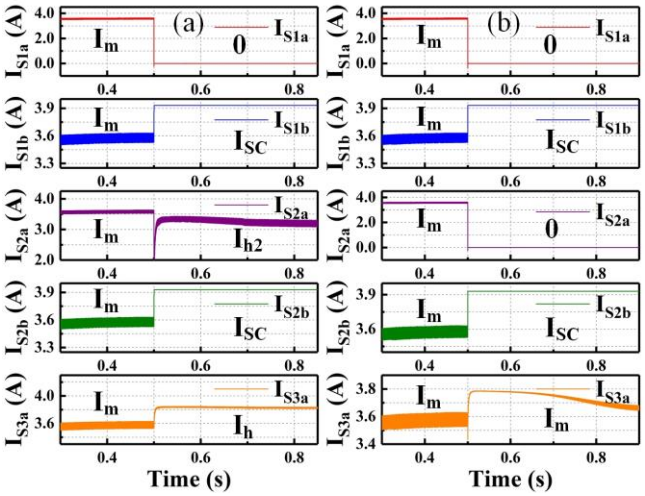

Fig. 7. The string currents at the occurrence of (a) P_1 is 75 %, P_2 is 87.5 %, and (b) P_1 is 50 %, P_2 is 62.5 %.

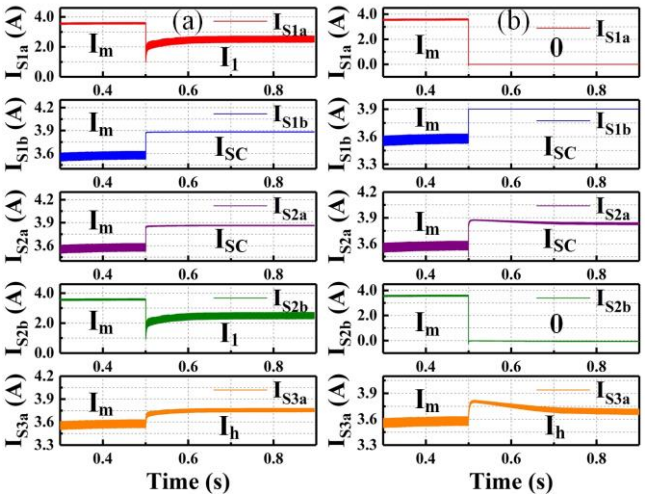

Fig. 8. The string currents at the occurrence of a CS LL fault (a) x = 4, y = 5, and (b) x = 4, y = 6.

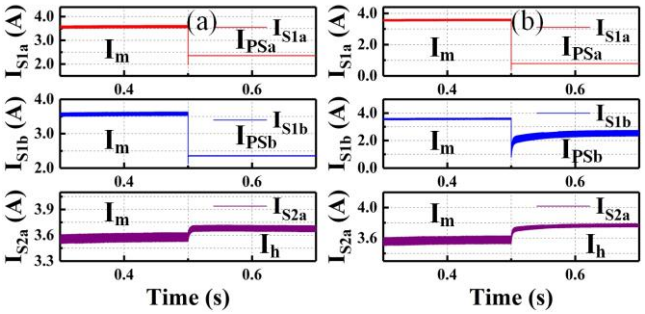

Fig. 9. The string currents when the first module of PVS1 is in the irradiance of (a) 300 and (b) 100 W/m^2.

shading. Initially, the single IS LL faults are examined at P = 87.5 % and P = 75 % of the PVS1. When the fault occurs at 0.5 s with the P of 87.5 %, the I_{S1a} is lower than I_m, I_{S1b} is I_{SC}, and I_{S2a} is I_h as shown in Fig. 6 (a). When the P is 75 %, PVS1 is open circuit and the healthy strings are operating at I_m as depicted in Fig. 6 (b). This is consistent with Eq. (4) that the PVS1 is open circuit when the P is less than 78.9 %.

The string currents at the double IS LL fault of PVS1 and PVS2 are shown in Fig. 7. When the P_1 is 75 % and P_2 is 87.5 %, the PVS1 is open circuit and PVS2 operates with current slightly lower than I_m as presented in Eq. (5) and (6). Due to LL faults, there are currents equal to I_{SC}. The string currents of healthy strings are larger than I_m as depicted in Fig. 7 (a). In the case that P_1 is 50 % and P_2 is 62.5 %, the two strings with LL faults are open circuit since they are lower than 75.87 % based on Eq. (6). The healthy strings are operating at MPP as depicted in Fig. 7 (b). The string currents at the CS LL fault with x = 4 and y = 5 are shown in Fig. 8 (a). In this case, the maximum value of I_1 is 2.45 A. According to Eq. (11), the difference between y and x should be less than 2; otherwise, the current I_1 becomes zero when x = 4 and y = 6 as depicted in Fig. 8 (b). It is confirmed that the currents of the second part of PVS1 and the first part of PVS2 are close to I_{SC}. The healthy strings are operating at the current larger than I_m as shown by the current at the beginning of PVS3 (I_{S3a}) in Fig. 8. In summary, the simulation results verify that the proposed model can detect and locate the LL faults.

The characteristics of partial shading are similar to an IS LL fault causing difficulties to the LL fault detection. The effects of partial shading on the string currents are studied with the PV system under the irradiance of 500 W/m^2. Due to the partial shading, the irradiance of the first module of PVS1 is decreased to 300 W/m^2 at 0.5 s. The I_{S1a} decreases to the current in partial shading (I_{PSa}) as shown in Fig. 9 (a). In this case, the irradiance is still high enough to sustain the operation of the first module of PVS1. Therefore, the I_{S1b} decreases to the current in partial shading (I_{PSb}) which is equal to I_{PSa}. The I_h is higher than I_m since the voltage of the PV system decreases to be lower than V_m. When the irradiance decreases to 100 W/m^2, the first module of PVS1 is unable to operate normally and most of the current passes through the bypass diode as depicted in Fig. 9 (b). The I_{S1a} decreases from I_m to I_{PSa}. Similarly, the I_h is larger than I_m. It can be seen that the string currents in partial shading are different from those under the IS LL fault conditions. The partial shading does not incur I_{SC}. Also, the currents at the beginning and terminal of a string are usually the same. They are different only when some shaded modules are not working and the currents of unshaded strings are higher than I_m. However, the I_h equals to I_m when the open circuit is caused by an IS LL fault as shown in Fig. 6 (b). Thus, it is validated that the proposed technique can detect the LL faults accurately despite the effects of partial shading.

V. Conclusion

The technique based on string-current behavior and current sensing has been developed for LL fault detection. The simulation results verified that the technique could achieve the detection of LL faults effectively despite the effects of MPPT, blocking diodes, and partial shading. In future work, the applicability of the technique will be further verified in a PV system with the MR sensors as the current sensors.

Acknowledgment

This work was supported in part by the Seed Funding Program for Basic Research, Seed Funding Program for Applied Research and Small Project Funding Program from The University of Hong Kong, Hong Kong, in part by the Innovation and Technology Fund (ITF) Tier 3 Funding under ITS/203/14, ITS/104/13, and ITS/214/14, in part by the Research Grants Council-General Research Fund (RGC-GRF) under Grant HKU 17204617, and in part by the University Grants Committee of Hong Kong under Contract AoE/P-04/08.

References

[1] A. Jäger-Waldau, "PV Status Report 2019," *European Commission*, 2019.
[2] D. S. Pillai et al., "A comprehensive review on protection challenges and fault diagnosis in PV systems," *Renewable and Sustainable Energy Reviews*, vol. 91, pp. 18-40, 2018.
[3] Y. Zhao et al., "Line–line fault analysis and protection challenges in solar photovoltaic arrays," *IEEE Trans. Ind. Electron.*, vol. 60, no. 9, pp. 3784-3795, 2013.
[4] J.-M. Huang et al., "Newly-Designed Fault Diagnostic Method for Solar Photovoltaic Generation System Based on IV-Curve Measurement," *IEEE Access*, 2019.
[5] W. Wang et al., "Fault diagnosis of photovoltaic panels using dynamic current–voltage characteristics," *IEEE Trans. Power Electron.*, vol. 31, no. 2, pp. 1588-1599, 2016.
[6] D. S. Pillai et al., "An MPPT based sensorless line-line and line-ground fault detection technique for PV systems," *IEEE Trans. Power Electron.*, vol. 34, no. 9, pp. 8646-8659, 2019.
[7] R. Hariharan et al., "A method to detect photovoltaic array faults and partial shading in PV systems," *IEEE J. Photovolt.*, vol. 6, no. 5, pp. 1278-1285, 2016.
[8] Y. Chaibi et al., "Simple and efficient approach to detect and diagnose electrical faults and partial shading in photovoltaic systems," *Energy Conversion and Management*, vol. 196, pp. 330-343, 2019.
[9] K. Ding et al., "A Health Status-Based Performance Evaluation Method of Photovoltaic System," *IEEE Access*, vol. 7, pp. 124055-124065, 2019.
[10] E. Garoudja et al., "Statistical fault detection in photovoltaic systems," *Solar Energy*, vol. 150, pp. 485-499, 2017.
[11] R. Platon et al., "Online fault detection in PV systems," *IEEE Trans. Sustain. Energy*, vol. 6, no. 4, pp. 1200-1207, 2015.
[12] Y. Zhao et al., "Graph-based semi-supervised learning for fault detection and classification in solar photovoltaic arrays," *IEEE Trans. Power Electron.*, vol. 30, no. 5, pp. 2848-2858, 2015.
[13] Z. Yi et al., "Line-to-line fault detection for photovoltaic arrays based on multiresolution signal decomposition and two-stage support vector machine," *IEEE Trans. Ind. Electron.*, vol. 64, no. 11, pp. 8546-8556, 2017.
[14] Z. Chen et al., "Deep residual network based fault detection and diagnosis of photovoltaic arrays using current-voltage curves and ambient conditions," *Energy Conversion and Management*, vol. 198, p. 111793, 2019.
[15] P. Jain et al., "A Digital Twin Approach for Fault Diagnosis in Distributed Photovoltaic System," *IEEE Trans. Power Electron.*, vol. 35, no. 1, pp. 940-956, 2020.
[16] P. Guerriero et al., "Monitoring and diagnostics of PV plants by a wireless self-powered sensor for individual panels," *IEEE J. Photovolt.*, vol. 6, no. 1, pp. 286-294, 2016.
[17] W. Miao et al., "Arc-Faults Detection in PV Systems by Measuring Pink Noise With Magnetic Sensors," *IEEE Trans. Magn.*, vol. 55, no. 7, pp. 1-6, 2019.
[18] A. Patel et al., "Current sensing for automotive electronics—A survey," *IEEE Trans. Veh. Technol.*, vol. 58, no. 8, pp. 4108-4119, 2009.